

Nearby SN-Associated GRB 190829A: Environment, Jet Structure, and VHE Gamma-Ray Afterglows

LU-LU ZHANG,¹ JIA REN,² XIAO-LI HUANG,² YUN-FENG LIANG,¹ DA-BIN LIN,¹ AND EN-WEI LIANG*¹

¹*Guangxi Key Laboratory for Relativistic Astrophysics, Department of Physics, Guangxi University, Nanning 530004, China;lew@gxu.edu.cn*

²*School of Astronomy and Space Science, Nanjing University, Nanjing 210023, China*

ABSTRACT

We present a self-consistent paradigm for interpreting the striking features of nearby low-luminosity GRB 190829A. Its prompt gamma-ray lightcurve has two separated pulses. We propose that the interaction of the hard prompt gamma-ray photons ($E_p = 624_{-303}^{+2432}$ keV) of its initial pulse with the dusty medium ($A_V = 2.33$) does not only result in the second soft gamma-ray pulse ($E_p \sim 12$ keV), but also makes a pre-accelerated e^\pm -rich medium shell via the $\gamma\gamma$ annihilation. In this paradigm, we show that the observed radio, optical, and X-ray afterglow lightcurves are well fit with the forward shock model. Its jet is almost isotropic ($\theta_j > 1.0$ rad) with a Lorentz factor of ~ 35 , and the electron density of the e^\pm -rich medium shell is ~ 15 cm⁻³, about 7 times higher than the electron density of its normal surrounding medium. The GRB ejecta catches up with and propagates into the e^\pm -rich medium shell at a region of $R = (4.07 - 6.46) \times 10^{16}$ cm, resulting in a bright afterglow bump at $\sim 10^3$ seconds post the GRB trigger. The predicted very high energy (VHE) gamma-ray emission from the synchrotron self-Compton process agrees with the H.E.S.S. observation. The derived broadband spectral energy distribution shows that GRB 190829A like nearby GRBs would be promising targets of the VHE gamma-ray telescopes, such as H.E.S.S., MAGIC, and CTA (Cherenkov Telescope Arrays).

Keywords: gamma-ray burst: general - gamma-ray burst: individual (GRB 190829A)

1. INTRODUCTION

As the most intense burst phenomena in the universe, gamma-ray bursts (GRBs) and their afterglows are theoretically predicted as sources of very high energy (VHE) gamma-rays and cosmic rays (Waxman 1995; Milgrom & Usov 1995; Vietri 1995; Abdalla et al. 2019; Samuelsson et al. 2020). They are listed as the target sources of current and future telescopes in the GeV-TeV gamma-ray bands. It is exciting that sub-TeV gamma-ray emission was firstly convincingly detected in the early afterglows of GRB 190114C with the Major Atmospheric Gamma Imaging Cerenkov Tele-

scopes (MAGIC; MAGIC Collaboration et al. 2019a). Its broad-band spectral energy distribution (SED) in the optical, X-ray, and gamma-ray bands can be well explained with the models of synchrotron radiation and synchrotron self-Compton (SSC) process of the electrons accelerated in the jet (MAGIC Collaboration et al. 2019b; Derishev & Piran 2019; Wang et al. 2019). The SSC component is also marginally detected in GRB 130427A (Liu et al. 2013; Ackermann et al. 2014; Joshi & Razzaque 2019; Huang et al. 2020a) and GRB 180720B (Fraija et al. 2019; Wang et al. 2019; Duan & Wang 2019). The window in the VHE gamma-ray band is opened for the GRB study. This is not only beneficial to reveal the radiation physics, but also critical for exploring the burst environment (e.g., Huang et al. 2020b).

Typical GRBs are happened at the high-redshift universe (Salvaterra 2015). VHE photons in the TeV-band are suffered sharply absorbed by the extragalactic background light (EBL) via the electron pair production (e.g., Stanev & Franceschini 1998; Dwek et al. 2005; Dwek & Krennrich 2005; Aharonian et al. 2006; Mazin & Raue 2007; Franceschini et al. 2008; Meyer et al. 2012; Fermi-LAT Collaboration et al. 2018). This is a great obstacle for the detection of VHE gamma-rays from typical GRBs. The detection of the VHE gamma-ray afterglow of GRB 190114C is some lucky since it is among the most energetic burst happened at a relatively low redshift ($z = 0.4245 \pm 0.0005$; Castro-Tirado et al. 2019). Note that nearby low-luminosity GRBs (LL-GRBs) seem to be a unique GRB population that is characterized by a high local event rate and large jet opening angle (e.g., Liang et al. 2007). It was proposed that they are considerable sources of VHE photons and cosmic rays (Murase 2019).

Interestingly, GRB 190829A is a LL-GRB associated with a broad-line type Ic supernova, SN 2019oyw (de Ugarte Postigo et al. 2019; Hu et al. 2020). It is among the nearest GRBs with a redshift of $z = 0.0785 \pm 0.005$ (Valeev et al. 2019). Its prompt gamma-rays have two distinct pulses, i.e., a hard-weak pulse followed by a soft-bright pulse with a separation of about 50 seconds (Chand et al. 2020), but the two pulses do not share the same $L_{\text{iso}} - E_p$ relation as usually seen in long GRBs (Lu et al. 2012). Its high energy afterglow was detected by H.E.S.S. at 4.3 hours after the GRB trigger (de Naurois & H. E. S. S. Collaboration 2019). Zhang et al. (2020) suggested that the VHE gamma-ray afterglow is produced in the external inverse-Compton scenario for seed photons supplied by the second emission episode of the prompt gamma-rays, but the bump have a long delay to the prompt gamma-rays. The optical and X-ray light curves of GRB 190829A afterglow have an achromatic bump with a rapid increase at around 700 seconds post the GRB trigger, and the X-ray afterglow faded as a single power-law up to more than 110 days without a detection of the jet break. The origin of the bump is uncertain. It was proposed that the bump may be due to the activity of the GRB central engine (Chand et al. 2020) or the dipole radiation of its remnant magnetar plus the forward shock emission (Fraija et al. 2020). Note that, similar optical afterglow bump was also observed in some GRBs, e.g., GRB 970508 (Castro-Tirado & Gorosabel 1999). Dai & Lu (2002) proposed that the bump is a signature of medium density jump. The radio afterglow of GRB 190829A was detected at an even later epoch than the X-ray afterglow and lasted longer (Rhodes et al. 2020). The interpretation of the radio afterglow is also debated. Rhodes et al. (2020) suggested that the radio afterglow in 15.5 GHz and 1.3 GHz is from the reverse and forward shocks, respectively. Sato et al. (2021) proposed that the observed low luminosity of GRB 190829A is due to the off-axis observation of a two-component jet and late X-ray and radio emissions are from the wide jet component.

In this paper, we revisit the data of GRB 190829A and present a self-consistent interpretation of its features mentioned above. We find that the radio, optical, X-ray afterglow data are well fitted with the forward shock model, and the VHE gamma-ray afterglow is resulted from the SSC process of the electrons in the jet without inducing an external seed photon field as proposed by Zhang et al. (2020). Our data analysis is present in § 2, and the afterglow light curve modeling is reported in § 3. We discuss the VHE emission of GRB 190829A afterglow in § 4. Conclusions and discussion on our results are presented in § 5.

2. DATA ANALYSIS

GRB 190829A was detected by *Fermi*/GBM, *Swift*/BAT, and *Konus*/Wind satellites (Lesage et al. 2019; Lien et al. 2019; Tsvetkova et al. 2019). Figure 1 shows its BAT light curve. It has two separated pulses. The spectrum of the first pulse in the 20 keV - 2 MeV range observed with *Konus*/Wind is well fitted with a power-law with exponential-cutoff model, yielding a photon index of $\alpha = -1.33_{-0.23}^{+0.30}$ and the peak photon energy of the νf_ν spectrum of $E_p = 624_{-303}^{+2432}$ keV in the burst rest frame (Tsvetkova et al. 2019). The second pulse is very soft and its spectrum observed with *Fermi*/GBM in the 8-1000 keV band can be fitted with a Band function (Band et al. 1993) with $E_p = 11.8 \pm 1.1$ keV in the burst rest frame, $\alpha = -0.92 \pm 0.62$, and $\beta = -2.51 \pm 0.01$ (Lesage et al. 2019).

We collect the afterglow data from the literature and GCN reports, and their light curves are shown in the left panel of Figure 2. Note that the optical light curve is shown with the data in u band taken from Chand et al. (2020) and Hu et al. (2020) since the data have good temporal coverage. The optical data has been corrected by extinctions from our Galaxy and the GRB host galaxy as discussed below. One can observe that the X-ray and optical light curves show the same behavior. They initially keep almost a constant and rapidly increase since $t > 700$ seconds and reach the peak at around $t = 1200$ seconds. The fluxes decay as normal afterglow from external shocks up to $\sim 10^7$ seconds in the X-ray band without the detection of jet break. Radio afterglows observed with the Meer Karoo Array Telescope (MeerKAT, 1.3 GHz, Monageng et al. 2019) and Arcminute Microkelvin Imager-Large Array (AMI-LA, 15.5 GHz) were detected from around one day to about 200 days post the GRB trigger (Rhodes et al. 2020). Note that the fluxes in the X-ray and 15.5 GHz band at $t > 5.5 \times 10^6$ seconds keep as constant, i.e., $F_X = 1.68 \times 10^{-13}$ erg cm $^{-2}$ s $^{-1}$ and $F_{15.5\text{GHz}} = 150$ μ Jy. They should be contributed by the GRB host galaxy. We subtract them from the X-ray flux and radio flux in the 15.5 GHz in our fitting of the light curves.

We make joint spectral analysis for the optical and X-ray band afterglows in the time interval $[3, 4] \times 10^4$ seconds. The X-ray data are observed with the *Swift*/XRT¹. The quasi-simultaneous optical g, r, i, z, J, H, K_s band data are taken from (Chen et al. 2019) and u band data is taken from Hu et al. (2020), as tabulated in their Table 3. All the optical data are corrected by the Galactic extinction (Schlafly & Finkbeiner 2011), and the Galactic HI column density is fixed at $N_{\text{H}}^{\text{Gal}} = 5.6 \times 10^{20}$ cm $^{-2}$. The extinction-law of the GRB host galaxy is taken the same as our Galaxy, i.e., $R_V = 3.08$ (Pei 1992). An absorbed power-law model is equated to fit the spectrum, yielding a HI column density of the GRB host galaxy at $z = 0.0785$ as $N_{\text{H}}^{\text{host}} = (5.79 \pm 0.53) \times 10^{21}$ cm $^{-2}$, the optimal color index as $E_{\text{B}-\text{V}} = 0.76 \pm 0.01$ corresponding to $A_V = R_V E_{\text{B}-\text{V}} = 2.33$. The photon index is 1.76 ± 0.01 . Our fit is shown in the right panel of Figure 2. Strong extinction indicates that the burst environment is

¹ Collected from https://www.swift.ac.uk/xrt_spectra/.

massively dusty. The u band data shown in Figure 2 are corrected with $A_u = 1.579$ (Schlegel et al. 1998).

3. A SELF-CONSISTENT PARADIGM AND MULTIWAVELENGTH AFTERGLOW MODELING

Basing on the data analysis above, we propose a paradigm to explain both the prompt and afterglow emission of GRB 190829A. We outline the paradigm as following. First, the ejecta powered by the central engine of GRB 190829A is quasi-isotropic since no jet break is detected later than 110 days post the GRB trigger. Second, the initial hard gamma-ray pulse is produced by internal shocks of the ejecta. Third, the hard gamma-ray photons ($E_p = 624_{-303}^{+2432}$ keV in the burst rest frame) are scattered by the density medium ($A_V = 2.33$), resulting the second soft gamma-ray pulse ($E_p = 11.8 \pm 1.1$ keV in the burst rest frame), similar to that proposed by Shao & Dai (2007). Forth, the interaction of the gamma-ray photons with the dust leads to an e^\pm -rich medium shell via the $\gamma\gamma$ annihilation, and the e^\pm -rich medium shell is also pre-accelerated by the gamma-ray photons (Madau & Thompson 2000; Thompson & Madau 2000; Mészáros et al. 2001; Beloborodov 2002, 2005; Beloborodov et al. 2014) before the front of the ejecta catching up with it. The observed optical and X-ray afterglow bump is due to the ejecta propagates into the e^\pm -rich medium shell. Fifth, the VHE gamma-ray afterglow observed with H.E.S.S. is produced via the SSC process.

In this paper, we do not calculate the gamma-ray scattering by the medium for producing the soft gamma-ray pulse, but focus on fitting the radio, optical and X-ray afterglow light curves within this paradigm with the standard forward shock model, in which the afterglow emission is attributed to the synchrotron radiation, synchrotron-self-Compton (SSC) scattering of relativistic electrons accelerated via external forward shocks (e.g., Fan et al. 2008; Ren et al. 2020). Moreover, the effect of equal-arrival-time surface is also considered in the calculations (Waxman 1997). The jet is assumed as a top-hat jet without lateral expansion (Huang et al. 1999). The synchrotron self-absorption, Klein-Nishina effect, and the $\gamma\gamma$ annihilation effects are also considered (e.g., Gould & Schröder 1967; Granot et al. 1999; Huang et al. 2020a; Zhang et al. 2020). We assume that the optical and X-ray bump since $t > 700$ seconds is due to the jet propagates into the e^\pm -rich medium, which is assumed to be a homogeneous shell with uniform density. Since the e^\pm -rich medium shell is resulted from the $\gamma\gamma$ annihilation, the dynamic evolution of the ejecta does not change before and after its propagation in the e^\pm -rich medium shell. We define the e^\pm -enriched shell with three parameters, R_s , R_e , and k , where R_s and R_e is the inner and outer boundary radius of the e^\pm -enriched shell, k is the lepton number density ratio of e^\pm -rich medium shell to the normal medium.

We use a Markov Chain Monte Carlo (MCMC) algorithm (emcee, Foreman-Mackey et al. 2013) to fit the multiwavelength light curves of GRB 190829A afterglow. Our result is shown in the left panel of Figure 2. One can observe that the light curves are well fitted with our model. The model light curve in 15.5 GHz has a similar bump feature in the early stage starting at ~ 700 seconds, but it has a long plateau up to 10^5 seconds. The model flux in the 1.3 GHz steady increases and peaks at 2×10^6 seconds.

The obtained parameters of jet and their 1σ confidence levels are shown as following: the isotropic kinetic energy $\log_{10} E_{k,iso}(\text{erg}) = 51.01_{-0.33}^{+0.43}$, the initial bulk Lorentz factor $\log_{10} \Gamma_0 = 1.55_{-0.33}^{+0.17}$, the circum-burst medium number density $\log_{10} n_0(\text{cm}^{-3}) = 0.34_{-0.70}^{+0.56}$, the electron energy fraction $\log_{10} \epsilon_e = -0.49_{-0.22}^{+0.46}$, the magnetic field energy fraction $\log_{10} \epsilon_B = -3.22_{-0.80}^{+1.21}$, and the spectrum in-

dex of electrons $p = 2.12_{-0.17}^{+0.08}$. The parameters of the e^\pm -rich shell are $\log_{10}R_s(\text{cm}) = 16.61_{-0.14}^{+0.30}$, $\log_{10}R_e(\text{cm}) = 16.81_{-0.15}^{+0.38}$, and $k = 6.87_{-2.55}^{+3.64}$.

Different from typical GRBs, the jet of GRB 190829A is middle relativistic, with $\Gamma_0 \sim 35$. No jet break is observed until $t > 5.5 \times 10^6$ seconds when the afterglow are dimmer than the host galaxy. Taking the jet break time $t_j > 5.5 \times 10^6$ seconds, we calculate the jet half-opening angle with (Frail et al. 2001)

$$\theta_j = 0.057 \left(\frac{t_j}{1\text{day}} \right)^{3/8} \left(\frac{1+z}{2} \right)^{-3/8} \left[\frac{E_{\gamma,\text{iso}}}{10^{53}\text{ergs}} \right]^{-1/8} \times \left(\frac{\eta_\gamma}{0.2} \right)^{1/8} \left(\frac{n}{0.1\text{cm}^{-3}} \right)^{1/8}, \quad (1)$$

where $E_{\gamma,\text{iso}}$, η_γ are the isotropic gamma-ray energy and radiative efficiency, respectively. The circum-burst medium density is taken as n_0 . The GRB efficiency is calculated as $\eta_\gamma = E_{\gamma,\text{iso}} / (E_{\gamma,\text{iso}} + E_{\text{k,iso}}) = 17\%$ with $E_{\gamma,\text{iso}} = 2 \times 10^{50}$ erg (Tsvetkova et al. 2019). We obtain $\theta_j > 1.0$ rad, indicating that the ejecta is almost isotropic.

4. VHE GAMMA-RAY AFTERGLOWS

H.E.S.S. detected the VHE gamma-rays of GRB 190829A afterglow with a confidence level of 5σ in the time interval from $t = T_0 + 4\text{h}20\text{m}$ to $t = T_0 + 7\text{h}54\text{m}$, but the observed flux is not released (de Naurois & H. E. S. S. Collaboration 2019)², where T_0 is the trigger time of *Fermi*/GBM. Therefore, our above afterglow modeling does not take the VHE gamma-ray afterglow into account. We examining whether our model calculation satisfies the observation with H.E.S.S., and presents a further discussion on whether it can be detectable with the current and near-future telescopes.

Figure 3 shows the 0.5 TeV and 0.2 - 4 TeV (H.E.S.S. energy band, H.E.S.S. Collaboration et al. 2021) lightcurves and the SEDs at 1200 seconds (the peak time of the light curve) and 2×10^4 seconds (in the time interval of H.E.S.S. observation for GRB 190829A). The light curve is corrected for the EBL absorption (Domínguez et al. 2011). One can find that VHE afterglow is very bright during the ejecta propagates in the e^\pm -rich shell. The afterglow light curve of GRB 190114C in the 0.5 TeV band is also shown in Figure 3 for comparison. One can find that flux of the VHE gamma-ray afterglow of GRB 190829A is comparable to GRB 190114C at the epoch from $[2 \times 10^3, 1 \times 10^4]$ seconds.

The SEDs illustrates that the $\gamma\gamma$ annihilation effect in the ejecta is considerable, especially in the early epoch. Taking the EBL absorption effects into account (Domínguez et al. 2011), the VHE afterglow at this time epoch are convincingly detectable with H.E.S.S., MAGIC and CTA (Cherenkov Telescope Arrays), but is not detectable with LHAASO (Large High Air Altitude Shower Observatory). The SED at $t = T_0 + 2 \times 10^4$ s shows that the VHE emission is still can be detectable with H.E.S.S., which is consistent with the observations (de Naurois & H. E. S. S. Collaboration 2019). It is also marginally detectable with MAGIC and convincingly detectable with CTA.

5. CONCLUSIONS AND DISCUSSION

We have revisited the multi-wavelength data of nearby LL-GRB 190829A and presented a self-consistent paradigm for interpreting its features by assuming an e^\pm -rich medium shell resulted from the interaction between the hard gamma-ray photons and dense medium pre-accelerated by the prompt gamma-rays. We show that the observed radio, optical, X-ray and VHE gamma-ray afterglows are attributed to the emission from the synchrotron radiation and the SSC process of the

² The H.E.S.S. observational data was published (H.E.S.S. Collaboration et al. 2021) when our manuscript is under reviewing. We also added the H.E.S.S. data in Figure 3.

electron accelerated in the forward shocks. The results of our fit to the multi-wavelength afterglow light curves show that the ejecta of GRB 190829A is almost isotropic ($\theta_j > 1.0$ rad) and middle relativistic ($\Gamma_0 \sim 35$). The electron density of the e^\pm -rich medium shell is $\sim 15 \text{ cm}^{-3}$, about 7 times higher than the electron density of its normal surrounding medium. Based on the model parameters derived in our analysis, we calculate the VHE gamma-ray light curve and the SED at the peak time of the light curve. It is found that its VHE gamma-ray emission is convincingly detectable with H.E.S.S., MAGIC, and CTA at its peak time.

The dusty medium should be essential for interpreting the data of GRB 190829A. The detection of associated SN 2019oyw with GRB 190829A confirms its progenitor as a massive star. Liang et al. (2007) proposed that local LL-GRBs would be a unique GRB population with low-luminosity, small beaming factor, and large local event rate. The ejecta of GRB 190829A is middle relativistic and quasi isotropic, being consistent with the features of the local LL-GRBs. Our joint optical-X-ray spectral analysis reveals that the ambient medium of the GRB is extremely dusty. By correcting i band SN data with a host galaxy extinction of $E_{B-V} = 0.757$ by assuming a Milky Way (MW) extinction law³, we find that the peak absolute magnitude of SN 2019oyw at i band is $M_i = -18.3 \pm 0.01$ mag, which is comparable to SN 2006aj ($M_i = -18.36 \pm 0.13$ mag) and SN 2010bh ($M_i = -18.58 \pm 0.08$ mag) (Hu et al. 2020).

We collect the A_V and N_H values of the GRBs associated with SN from literature, as reported in Table 1. Figure 4 shows N_H as a function of A_V . A sample of typical long GRBs taken from literature, together with the typical dust-to-gas ratio for the local group (LG) environment $N_H/A_V = 1.6 \times 10^{22} \text{ cm}^{-2} \text{ mag}^{-1}$ (Covino et al. 2013), is also shown in Figure 4. One can observe that the A_V value of GRB 190829A is the largest one among the SN-associated GRB sample, although it is still not significantly distinct from the typical GRBs. It closes to the dust-to-gas ratio for the LG environment, but is above the ratio as most long GRBs.

It was proposed that the interaction between the prompt gamma-ray pulse and the medium not only can pre-accelerate the ambient medium to a high Lorentz factor, but also accompany by e^\pm loading via the pair production process (e.g., Thompson & Madau 2000; Madau & Thompson 2000; Mészáros et al. 2001). This may affect the GRB afterglow behaviors (e.g., Beloborodov 2002). We suspect that the e^\pm -rich medium shell is resulted from the interaction of the initial extremely hard gamma-ray photons of GRB 190829A with the dusty medium ($A_V = 2.33$). As proposed by Shao & Dai (2007), the dust scattering of the gamma-ray photons may lead to softening echo emission. This may naturally explain the observed soft gamma-ray pulse with a time decay of 50 seconds with respect to the first gamma-ray pulse. We compare them in the inset of Figure 1 by normalizing their flux levels and making alignment with respect to the starting time of the two pulses. It is find that their initial rising parts are similar, but the second pulse is more symmetric than the first pulse with a FWHM about twice of the first pulse. It is possible that the symmetric feature may be due to echo emission during scattering.

Because the e^\pm -rich medium shell is formed at 50 second post the first pulse, the observed time decay of afterglow bump is $\sim 10^3$ seconds. Our fit indicates that the e^\pm -rich medium shell is at a region of $R = (4.07 - 6.46) \times 10^{16}$ cm. This is generally consistent with the forward shock region for the GRB afterglows (Mu et al. 2016). The time delay for the ejecta catching up with the e^\pm -rich

³ The E_{B-V} value reported in Chand et al. (2020) is 1.04 by adopting a the Small Magellanic Cloud (SMC) extinction law. Besides, the difference in time interval selection for joint spectral fit may also lead to derive different extinction value.

medium shell is estimated as $\Delta t = R/c\Gamma_0^2 \simeq 1.1 \times 10^3$ seconds without considering the deceleration of the ejecta⁴. This is consistent with the observation.

ACKNOWLEDGMENTS

We acknowledge the use of the public data from the *Swift* data archive and the UK *Swift* Science Data Center. This research has made use of the CTA instrument response functions provided by the CTA Consortium and Observatory, see <http://www.cta-observatory.org/science/cta-performance/> (version prod3b-v2) for more details. This work is supported by the National Natural Science Foundation of China (Grant No.11533003, 11851304, and U1731239) and Guangxi Science Foundation (grant No. 2017AD22006).

⁴ The ejecta may move in a cavity since the medium is pre-accelerated by the prompt gamma-rays (Beloborodov 2002).

REFERENCES

- Abdalla, H., Adam, R., Aharonian, F., et al. 2019, *Nature*, 575, 464, doi: [10.1038/s41586-019-1743-9](https://doi.org/10.1038/s41586-019-1743-9)
- Ackermann, M., Ajello, M., Asano, K., et al. 2014, *Science*, 343, 42, doi: [10.1126/science.1242353](https://doi.org/10.1126/science.1242353)
- Aharonian, F., Akhperjanian, A. G., Bazer-Bachi, A. R., et al. 2006, *Nature*, 440, 1018, doi: [10.1038/nature04680](https://doi.org/10.1038/nature04680)
- Bai, X., Bi, B. Y., Bi, X. J., et al. 2019, arXiv e-prints, arXiv:1905.02773. <https://arxiv.org/abs/1905.02773>
- Band, D., Matteson, J., Ford, L., et al. 1993, *ApJ*, 413, 281, doi: [10.1086/172995](https://doi.org/10.1086/172995)
- Beloborodov, A. M. 2002, *ApJ*, 565, 808, doi: [10.1086/324195](https://doi.org/10.1086/324195)
- . 2005, *ApJ*, 627, 346, doi: [10.1086/430166](https://doi.org/10.1086/430166)
- Beloborodov, A. M., Hascoët, R., & Vurm, I. 2014, *ApJ*, 788, 36, doi: [10.1088/0004-637X/788/1/36](https://doi.org/10.1088/0004-637X/788/1/36)
- Cano, Z., de Ugarte Postigo, A., Perley, D., et al. 2015, *MNRAS*, 452, 1535, doi: [10.1093/mnras/stv1327](https://doi.org/10.1093/mnras/stv1327)
- Castro-Tirado, A. J., & Gorosabel, J. 1999, *A&AS*, 138, 449, doi: [10.1051/aas:1999303](https://doi.org/10.1051/aas:1999303)
- Castro-Tirado, A. J., Hu, Y., Fernandez-Garcia, E., et al. 2019, *GRB Coordinates Network*, 23708, 1
- Chand, V., Banerjee, A., Gupta, R., et al. 2020, *ApJ*, 898, 42, doi: [10.3847/1538-4357/ab9606](https://doi.org/10.3847/1538-4357/ab9606)
- Chen, T. W., Bolmer, J., Nicuesa Guelbenzu, A., & Klose, S. 2019, *GRB Coordinates Network*, 25569, 1
- Covino, S., Melandri, A., Salvaterra, R., et al. 2013, *MNRAS*, 432, 1231, doi: [10.1093/mnras/stt540](https://doi.org/10.1093/mnras/stt540)
- Dai, Z. G., & Lu, T. 2002, *ApJL*, 565, L87, doi: [10.1086/339418](https://doi.org/10.1086/339418)
- de Naurois, M., & H. E. S. S. Collaboration. 2019, *GRB Coordinates Network*, 25566, 1
- de Ugarte Postigo, A., Izzo, L., Thoene, C. C., et al. 2019, *GRB Coordinates Network*, 25677, 1
- Derishev, E., & Piran, T. 2019, *ApJL*, 880, L27, doi: [10.3847/2041-8213/ab2d8a](https://doi.org/10.3847/2041-8213/ab2d8a)
- Domínguez, A., Primack, J. R., Rosario, D. J., et al. 2011, *MNRAS*, 410, 2556, doi: [10.1111/j.1365-2966.2010.17631.x](https://doi.org/10.1111/j.1365-2966.2010.17631.x)
- Duan, M.-Y., & Wang, X.-G. 2019, *ApJ*, 884, 61, doi: [10.3847/1538-4357/ab3c6e](https://doi.org/10.3847/1538-4357/ab3c6e)
- Dwek, E., & Krennrich, F. 2005, *ApJ*, 618, 657, doi: [10.1086/426010](https://doi.org/10.1086/426010)
- Dwek, E., Krennrich, F., & Arendt, R. G. 2005, *ApJ*, 634, 155, doi: [10.1086/462400](https://doi.org/10.1086/462400)
- Fan, Y.-Z., Piran, T., Narayan, R., & Wei, D.-M. 2008, *MNRAS*, 384, 1483, doi: [10.1111/j.1365-2966.2007.12765.x](https://doi.org/10.1111/j.1365-2966.2007.12765.x)
- Fermi-LAT Collaboration, Abdollahi, S., Ackermann, M., et al. 2018, *Science*, 362, 1031, doi: [10.1126/science.aat8123](https://doi.org/10.1126/science.aat8123)
- Foreman-Mackey, D., Hogg, D. W., Lang, D., & Goodman, J. 2013, *PASP*, 125, 306, doi: [10.1086/670067](https://doi.org/10.1086/670067)
- Fraija, N., Veres, P., Beniamini, P., et al. 2020, arXiv e-prints, arXiv:2003.11252. <https://arxiv.org/abs/2003.11252>
- Fraija, N., Dichiara, S., Pedreira, A. C. C. d. E. S., et al. 2019, *ApJ*, 885, 29, doi: [10.3847/1538-4357/ab3e4b](https://doi.org/10.3847/1538-4357/ab3e4b)
- Frail, D. A., Kulkarni, S. R., Sari, R., et al. 2001, *ApJL*, 562, L55, doi: [10.1086/338119](https://doi.org/10.1086/338119)
- Franceschini, A., Rodighiero, G., & Vaccari, M. 2008, *A&A*, 487, 837, doi: [10.1051/0004-6361:200809691](https://doi.org/10.1051/0004-6361:200809691)
- Granot, J., Piran, T., & Sari, R. 1999, *ApJ*, 527, 236, doi: [10.1086/308052](https://doi.org/10.1086/308052)
- Gould, R. J., & Schröder, G. P. 1967, *Physical Review*, 155, 1404, doi: [10.1103/PhysRev.155.1404](https://doi.org/10.1103/PhysRev.155.1404)
- H.E.S.S. Collaboration, Abdalla, H., Aharonian, F., et al. 2021, *Science*, 372, 1081, doi: [10.1126/science.abe8560](https://doi.org/10.1126/science.abe8560)
- Hu, Y. D., Castro-Tirado, A. J., Kumar, A., et al. 2020, arXiv e-prints, arXiv:2009.04021. <https://arxiv.org/abs/2009.04021>
- Huang, X.-L., Liang, E.-W., Liu, R.-Y., Cheng, J.-G., & Wang, X.-Y. 2020a, *ApJL*, 903, L26, doi: [10.3847/2041-8213/abc330](https://doi.org/10.3847/2041-8213/abc330)
- Huang, X.-L., Wang, Z.-R., Liu, R.-Y., Wang, X.-Y., & Liang, E.-W. 2020b, arXiv e-prints, arXiv:2012.13313. <https://arxiv.org/abs/2012.13313>
- Huang, Y. F., Dai, Z. G., & Lu, T. 1999, *MNRAS*, 309, 513, doi: [10.1046/j.1365-8711.1999.02887.x](https://doi.org/10.1046/j.1365-8711.1999.02887.x)
- Joshi, J. C., & Razzaque, S. 2019, arXiv e-prints, arXiv:1911.01558. <https://arxiv.org/abs/1911.01558>

- Lesage, S., Poolakkil, S., Fletcher, C., et al. 2019, GRB Coordinates Network, 25575, 1
- Li, L., Wang, Y., Shao, L., et al. 2018, *ApJS*, 234, 26, doi: [10.3847/1538-4365/aaa02a](https://doi.org/10.3847/1538-4365/aaa02a)
- Liang, E.-W., Zhang, B.-B., & Zhang, B. 2007, *ApJ*, 670, 565, doi: [10.1086/521870](https://doi.org/10.1086/521870)
- Lien, A. Y., Barthelmy, S. D., Cummings, J. R., et al. 2019, GRB Coordinates Network, 25579, 1
- Liu, R.-Y., Wang, X.-Y., & Wu, X.-F. 2013, *ApJL*, 773, L20, doi: [10.1088/2041-8205/773/2/L20](https://doi.org/10.1088/2041-8205/773/2/L20)
- Lu, R.-J., Wei, J.-J., Liang, E.-W., et al. 2012, *ApJ*, 756, 112, doi: [10.1088/0004-637X/756/2/112](https://doi.org/10.1088/0004-637X/756/2/112)
- Madau, P., & Thompson, C. 2000, *ApJ*, 534, 239, doi: [10.1086/308738](https://doi.org/10.1086/308738)
- MAGIC Collaboration, Acciari, V. A., Ansoldi, S., et al. 2019a, *Nature*, 575, 455, doi: [10.1038/s41586-019-1750-x](https://doi.org/10.1038/s41586-019-1750-x)
- . 2019b, *Nature*, 575, 459, doi: [10.1038/s41586-019-1754-6](https://doi.org/10.1038/s41586-019-1754-6)
- Mazin, D., & Raue, M. 2007, *A&A*, 471, 439, doi: [10.1051/0004-6361:20077158](https://doi.org/10.1051/0004-6361:20077158)
- Mészáros, P., Ramirez-Ruiz, E., & Rees, M. J. 2001, *ApJ*, 554, 660, doi: [10.1086/321404](https://doi.org/10.1086/321404)
- Meyer, M., Raue, M., Mazin, D., & Horns, D. 2012, *A&A*, 542, A59, doi: [10.1051/0004-6361/201118284](https://doi.org/10.1051/0004-6361/201118284)
- Milgrom, M., & Usov, V. 1995, *ApJL*, 449, L37, doi: [10.1086/309633](https://doi.org/10.1086/309633)
- Monageng, I., van der Horst, A. J., Woudt, P. A., Bottcher, M., & et al. 2019, GRB Coordinates Network, 25635, 1
- Mu, H.-J., Lin, D.-B., Xi, S.-Q., et al. 2016, *ApJ*, 831, 111, doi: [10.3847/0004-637X/831/1/111](https://doi.org/10.3847/0004-637X/831/1/111)
- Murase, K. 2019, in International Cosmic Ray Conference, Vol. 36, 36th International Cosmic Ray Conference (ICRC2019), 965. <https://arxiv.org/abs/1912.05764>
- Pei, Y. C. 1992, *ApJ*, 395, 130, doi: [10.1086/171637](https://doi.org/10.1086/171637)
- Ren, J., Lin, D.-B., Zhang, L.-L., et al. 2020, *ApJL*, 901, L26, doi: [10.3847/2041-8213/abb672](https://doi.org/10.3847/2041-8213/abb672)
- Rhoads, J. E., & Fruchter, A. S. 2001, *ApJ*, 546, 117, doi: [10.1086/318246](https://doi.org/10.1086/318246)
- Rhodes, L., van der Horst, A. J., Fender, R., et al. 2020, *MNRAS*, 496, 3326, doi: [10.1093/mnras/staa1715](https://doi.org/10.1093/mnras/staa1715)
- Salvaterra, R. 2015, *Journal of High Energy Astrophysics*, 7, 35, doi: [10.1016/j.jheap.2015.03.001](https://doi.org/10.1016/j.jheap.2015.03.001)
- Samuelsson, F., Bégué, D., Ryde, F., Pe'er, A., & Murase, K. 2020, *ApJ*, 902, 148, doi: [10.3847/1538-4357/abb60c](https://doi.org/10.3847/1538-4357/abb60c)
- Sato, Y., Obayashi, K., Yamazaki, R., Murase, K., & Ohira, Y. 2021, arXiv e-prints, arXiv:2101.10581. <https://arxiv.org/abs/2101.10581>
- Schlaflly, E. F., & Finkbeiner, D. P. 2011, *ApJ*, 737, 103, doi: [10.1088/0004-637X/737/2/103](https://doi.org/10.1088/0004-637X/737/2/103)
- Schlegel, D. J., Finkbeiner, D. P., & Davis, M. 1998, *ApJ*, 500, 525, doi: [10.1086/305772](https://doi.org/10.1086/305772)
- Shao, L., & Dai, Z. G. 2007, *ApJ*, 660, 1319, doi: [10.1086/513139](https://doi.org/10.1086/513139)
- Stanev, T., & Franceschini, A. 1998, *ApJL*, 494, L159, doi: [10.1086/311183](https://doi.org/10.1086/311183)
- Suzuki, A., Maeda, K., & Shigezawa, T. 2019, *ApJ*, 870, 38, doi: [10.3847/1538-4357/aaef85](https://doi.org/10.3847/1538-4357/aaef85)
- Thompson, C., & Madau, P. 2000, *ApJ*, 538, 105, doi: [10.1086/309100](https://doi.org/10.1086/309100)
- Tsvetkova, A., Golenetskii, S., Aptekar, R., et al. 2019, GRB Coordinates Network, Circular Service, No. 25660, 25660
- Valeev, A. F., Castro-Tirado, A. J., Hu, Y. D., et al. 2019, GRB Coordinates Network, 25565, 1
- Vietri, M. 1995, *ApJ*, 453, 883, doi: [10.1086/176448](https://doi.org/10.1086/176448)
- Wang, X.-Y., Liu, R.-Y., Zhang, H.-M., Xi, S.-Q., & Zhang, B. 2019, *ApJ*, 884, 117, doi: [10.3847/1538-4357/ab426c](https://doi.org/10.3847/1538-4357/ab426c)
- Waxman, E. 1995, *PhRvL*, 75, 386, doi: [10.1103/PhysRevLett.75.386](https://doi.org/10.1103/PhysRevLett.75.386)
- . 1997, *ApJL*, 491, L19, doi: [10.1086/311057](https://doi.org/10.1086/311057)
- Zhang, B. T., Murase, K., Veres, P., & Mészáros, P. 2020, arXiv e-prints, arXiv:2012.07796. <https://arxiv.org/abs/2012.07796>

Table 1. Properties of the GRB-SN Samples with Multicolor Light Curves

GRB/SN	Redshift	A_V^{host} (mag) ^a	N_{H} (10^{21} cm) ^d	T (s)
980425/1998bw	0.0085	0.17 ± 0.02	—	—
030329/2003dh	0.16867	0.39 ± 0.15	—	—
050525A/2005nc	0.606	0.36 ± 0.05	$5.9_{-2.7}^{+3.6}$	$T_0 + 151542$
060218/2006aj	0.03342	0.13 ± 0.01	$3.1_{-0.6}^{+0.7}$	$T_0 + 7028$
081007/2008hw	0.5295	0.31 ± 0.25	$7.7_{-1.4}^{+1.5}$	$T_0 + 8027$
091127/2009nz	0.49044	0.17 ± 0.15	$1.1_{-0.6}^{+0.6}$	$T_0 + 13229$
100316D/2010bh	0.0592	0.43 ± 0.03	20_{-11}^{+16}	$T_0 + 133397$
101219B/2010ma	0.55185	< 0.1	$0.7_{-0.5}^{+0.6}$	$T_0 + 362754$
111209A/2011kl	0.677	0.3 ± 1.5	$2.7_{-0.8}^{+0.8}$	$T_0 + 267284$
130427A/2013c	0.3399	0.13 ± 0.06	$1.22_{-0.18}^{+0.18}$	$T_0 + 712132$
130702A/2013dx	0.677	0.3 ± 0.07	$1.4_{-0.3}^{+0.31}$	$T_0 + 1478125$
130831A/2013fu	0.4791	0.06 ± 0.04	$0.2_{-0.2}^{+3.88}$	$T_0 + 251766$
140606B/iPTF14bfu	0.384	0.47 ± 0.41^b	6_{-5}^{+8}	$T_0 + 187980$
171205A/2017iuk	0.0368	0.155^c	$1.2_{-0.7}^{+0.8}$	$T_0 + 749534$
190829A/2019oyw	0.0785	2.33	$5.79_{-0.53}^{+0.53}$	$T_0 + (3 - 4) \times 10^4$

^aThe values of A_V , redshift z from GRB 980425 to GRB 130831A are taken from Li et al. (2018), except for 140606B/iPTF14bfu from Cano et al. (2015)^b and 171205A/2017iuk from Suzuki et al. (2019)^c.

^dTaken from the XRT Catalogue entry of *Swift* website and T is the corresponding time for extracting the XRT spectrum.

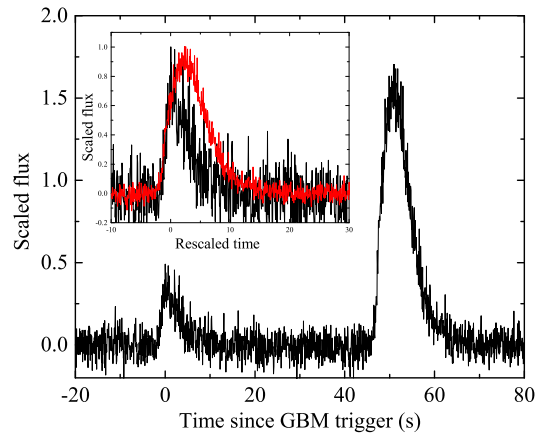


Figure 1. Prompt gamma-ray light curve of GRB 190829A observed with *Fermi*/GBM. The inset shows the comparison of the two gamma-ray pulses by re-scaling their flux level and making alignment of their beginning times.

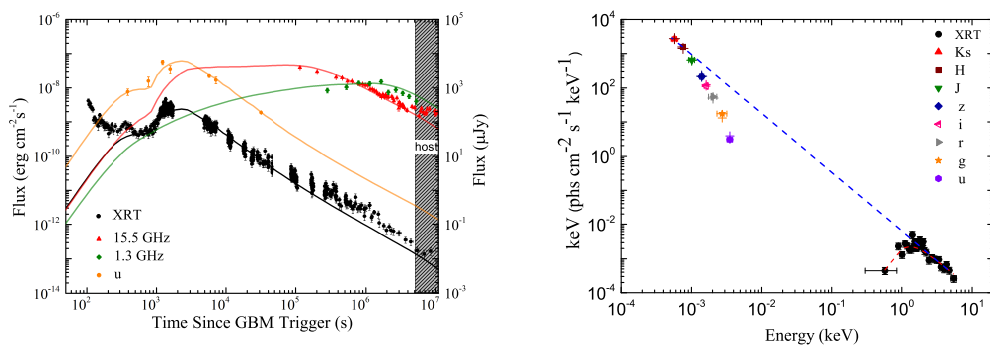


Figure 2. *Left panel*— Multiwavelength afterglow lightcurves (dots) of GRB 190829A along with our fits with the forward shock model (lines). The shaded region marks the afterglows are dimmer than the emission of the host galaxy. *Right panel*— Joint optical-X-ray afterglow spectrum (dots) observed in the time interval of $[3, 4] \times 10^4$ s of GRB 190829A along with our fit with a single power-law function (dashed lines). The optical data are extinction-corrected for our Galaxy only. Extinction and HI absorption of both our Galaxy and the GRB host galaxy are considered in our spectral fit.

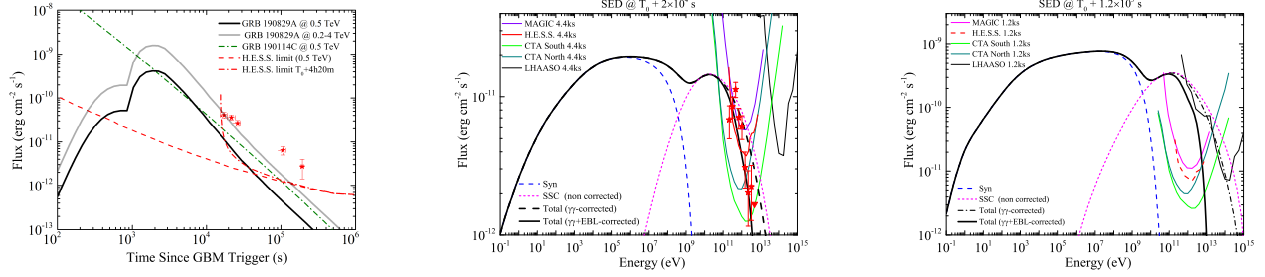


Figure 3. *Left panel*— The theoretical lightcurves at 0.5 TeV (black solid line) and in the H.E.S.S. energy band (0.2 - 4 TeV, gray solid line) of GRB 190829A. The H.E.S.S. data taken from (H.E.S.S. Collaboration et al. 2021) are shown with red stars. The theoretical 0.5 TeV lightcurve of GRB 190114C (green dash-dotted line) is also shown for comparison. The $\gamma\gamma$ annihilation in the ejecta and EBL absorption are corrected. The sensitivity curves at 0.5 TeV of H.E.S.S. starting from the *Fermi*/GBM trigger time T_0 and starting from $T_0 + 4\text{h}20\text{m}$ are shown in red dashed line and red dash-dotted line, respectively. *Middle and Right panels*— The numerical SEDs of GRB 190829A at 2×10^4 s and 1200 s, respectively. The H.E.S.S. data observed in the time interval [4.5, 7.9] hours taken from (H.E.S.S. Collaboration et al. 2021) are shown with red stars. The sensitivity curves scaled to an observational times of 2×10^4 s and 1200 s are also shown. The sensitivity curves are adopted from Bai et al. (2019) and <https://www.cta-observatory.org/science/cta-performance/>.

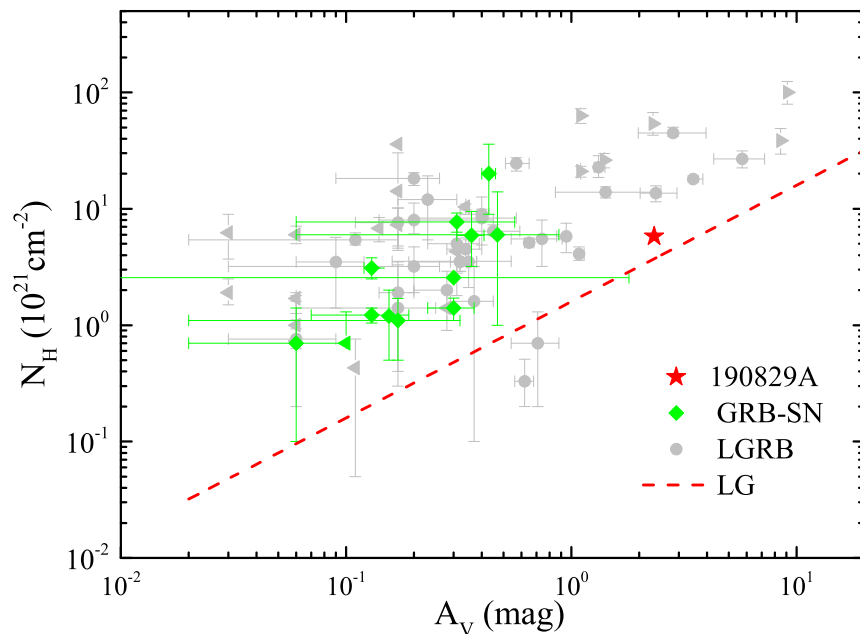


Figure 4. N_{H} as a function of A_{V} of GRBs associated with an associated SNe (green diamond dots) in comparison with typical long GRBs (grey dots and triangles) from Covino et al. (2013). Triangle represents the upper or lower limit. GRB 190829A-SN 2019oyw is marked as red star. The red dashed line shows typical dust-to-gas ratio for the local group (LG) environment (Covino et al. 2013).